

# **Instrument calibration of the Hayabusa near-infrared spectrometer**

Masanao Abe

Institute of Space and Astronautical Science  
Japan Aerospace Exploration Agency  
3-1-1 Yoshinodai, Sagamihara  
Kanagawa 229-8510, Japan

Yasuhiko Takagi

Aichi Toho University  
3-11 Heiwagaoka, Meito-ku  
Nagoya 465-8515, Japan

Shinsuke Abe

Institute of Astronomy  
National Central University  
300 Jhongda Rd, Jhongli  
Taoyuan 32001, Taiwan

Kohei Kitazato

Department of Earth and Planetary Sciences  
Kobe University  
1-1 Rokkodai, Nada-ku  
Kobe 657-8501, Japan

26 Manuscript Pages

9 Figures

1 Tables

**Proposed Running Head:** Hayabusa NIRS calibration

Corresponding Author:

Masanao Abe

Institute of Space and Astronautical Science

Japan Aerospace Exploration Agency

3-1-1 Yoshinodai, Sagamihara

Kanagawa 229-8510, Japan

Phone: +81-42-759-8189

Fax: +81-42-759-8457

Email: [abe@planeta.sci.isas.jaxa.jp](mailto:abe@planeta.sci.isas.jaxa.jp)

## **Abstract**

The Hayabusa Near-Infrared Spectrometer (NIRS) performed a comprehensive series of in-flight tests to validate its preflight radiometric characteristics and to characterize instrument stability, pointing, and co-alignment with other instruments under flight conditions. The results of these tests form the basis of the NIRS data reduction and calibration procedure and should support the ability of NIRS to achieve its science goal of spectrally mapping Hayabusa's target asteroid, 25143 Itokawa. Main results include the following: (1) Radiometric calibration of NIRS has been confirmed to be accurate to within 5%, based on NIRS measurements of astronomical targets and comparisons to radiances derived from the ground-based optical instruments; (2) The radiometric response had been stable on the scale of months and the gradual changes in detector sensitivity over 2 years of operations in space may have been demonstrated by slight displacement of the detector arrays; (3) The unexpected stray lights on NIRS spectra were characterized by in-flight experiences; (4) The co-alignment of NIRS with respect to the other Hayabusa instruments has been determined.

**Key Words:** instrumentation; asteroids, composition; spectroscopy; Hayabusa

## 1. Introduction

The Near-Infrared Spectrometer (NIRS) instrument on the Hayabusa had acquired more than 80,000 spatial-resolved spectra of the asteroid Itokawa through the rendezvous operation. The primary objectives of NIRS investigations include mapping the composition and distribution of surface minerals at spatial resolutions as high as a few ten meters based on diagnostic absorption features of the rock-forming minerals (Abe et al., 2006). NIRS data complement high-resolution images from the multiband imaging camera (AMICA) (Saito et al., 2006), and low spatial resolution elemental distribution from the X-ray spectrometer (XRS) (Okada et al., 2006) for identification of the materials composing Itokawa's surface. This information together would constrain the history of geologic processes that formed the asteroid, and determine the links between materials composing the asteroid and their meteorite analogs.

The Hayabusa spacecraft was successfully launched by the fifth Mu V launch vehicle on May 9, 2003. After the one-year orbital loop around the Sun, the spacecraft returned to Earth for a close flyby on May 20, 2004, obtaining a gravity assist that raises the heliocentric orbit energy and changes the orbital inclination. During the Earth flyby, Hayabusa passed within 3700 km of Earth's surface and the onboard instruments performed observations of the Earth and Moon. More than one-year later, on September 12, 2005, Hayabusa reached the target asteroid Itokawa and begun three-month rendezvous operations. Currently, the spacecraft has been planned to return to Earth in 2010.

Successfully achieving the scientific goals requires a high degree of accuracy and precision in the calibration of NIRS spectra. A calibration was derived for NIRS based on extensive preflight laboratory measurements. During flight operations leading up to Itokawa, we acquired additional in-flight calibration data that have allowed us to augment, extend, and enhance the quality of calibrated NIRS spectra. This paper describes the methods and results for these NIRS calibration activities, and provides the instrumental and data set information. The raw NIRS spectral data observed during the flight and rendezvous operations have been archived and distributed through the JAXA's Hayabusa Science Data Archive (<http://darts.isas.jaxa.jp/planet/project/hayabusa/>).

## 2. Instrument Description

The NIRS is composed of a grating infrared spectrometer (NIRS-S), a spectrometer electronics (NIRS-E) and a data processing unit to control NIRS, which is also used to operate the Hayabusa XRS. The NIRS-S is mounted on -Y panel inside surface of the

spacecraft chassis in such a way that the viewing is fixed in almost the spacecraft  $-Z$  axis, direction in which opposite the solar arrays and high-gain antenna (see Fujiwara et al., 2000).

The NIRS optical design, summarized in Figure 1, consists of an entrance aperture stop, a field stop slit, two mirrors, a diffraction grating, a camera lens assembly, a detector, and two calibration targets. The assembled spectrometer is covered with carbon-fiber reinforced plastic box case ( $300 \times 150 \times 100$  mm in size). After passing through the slit, incident light is dispersed by a grism, transmission diffraction grating, combined with a cross disperser and re-imaged off by a camera optics. The first-order light fall on a 64-element indium-gallium-arsenide (InGaAs) linear detector array that covers the range of 750-2250 nm, in increments of 24 nm. The cross disperser prevents light other than first-order from reaching the detector. NIRS carries the two types of onboard calibration targets, an incandescent halogen lamp and a light-emitting-diode (LED), for periodic monitoring of detector stability. These targets are mounted on the aperture plate. The design was developed in accordance with the requirements of downsizing and weight saving.

Table 1 lists key specifications and characteristics of the instrument. Note that the calibration LED is fixed outside of aperture but the lamp is fixed on the inner edge of aperture so that the effective aperture size drop off by  $\sim 4\%$ . The slit size was determined as it can provide an angular field-of-view (FOV) of  $0.1^\circ \times 0.1^\circ$ , which corresponds to the spatial resolution of  $17 \text{ m} \times 17 \text{ m}$  at a distance of 10 km. A moveable shutter can be used to block completely the slit for dark current measurements. The signal in a dark spectrum represents the background electronic and other noise inherent in the instrument. A thermoelectric Peltier device actively cools the InGaAs detector arrays in order to achieve a sufficient signal-to-noise ratio (SNR). The detector has a built-in complementary-metal-oxide-semiconductor (CMOS) image sensor, which is used to multiplex the outputs to a single analog to digital (A/D) converter.

### **3. Operating Modes and Data Acquisition**

NIRS operation modes are implemented in the onboard software using instrument parameters that can be changed by ground operation commands. There are a total of five modes available to NIRS; NORMAL, RAW, HIST, LIDAR, and FLASH.

In the NORMAL mode, each observation consists of certain sequential sets of alternate light and dark frames (see Figure 2). That is accomplished by chopping-motion of the shutter, allowing the dark current level of the detector to be subtracted on a channel-by-channel basis every time. The CMOS image sensor serves to read differences of outputs on each detector

element between light and dark frames. The NIRS frame length is 65.536 ms, which corresponds to half of the shutter driving cycle, and exposure time can be changed at 256-stage from 0.256 ms to 57.344 ms. In addition, the number of stacked light-dark frame set can be also changed from 1 to  $2^{255}$  as n-th power of two. Most of NIRS data were taken in this mode.

The basic unit of spectral data for any given NIRS channel is digital number (DN) showing the integrated photon counts during a setting exposure-time interval. The raw data are originally sampled with 14 bits per channel (0-16383 DNs). A DN has a value of approximately 0.565 mV output from the detector pre-amplifiers when at gain  $1.08 \times$ . In the NORMAL mode, the data averaging of light frames subtracted dark spectrum are operated with onboard software, and only the mean, deviation, maximum and minimum of the DNs at individual channels were downloaded in instrument telemetry. The RAW mode prohibits the data averaging on board the spacecraft. The HIST mode provides a sequential output of the housekeeping (HK) data for NIRS. However, the RAW and HIST modes have not been used in reality until the completion of the asteroid observation.

The LIDAR and FLASH modes were supposed to be used in the descent and touchdown phase during the Hayabusa rendezvous with Itokawa. In the LIDAR mode, NIRS carries out the frame difference readout in sync with the periodic laser pulse of LIDAR (a laser ranging instrument on the Hayabusa) so as to observe the reflected laser light of the LIDAR from the asteroid surface. The shutter stays open during this observation mode. On the other hand, the FLASH mode was designed to remove the frame contaminated by flashlights to irradiate target markers for autonomous navigation of sampling. This mode is identical to the NORMAL mode, excluding the removal of the synchronized frame with flashlights.

#### **4. Pre-launch Calibration and Characterization**

The NIRS instrument was tested and calibrated extensively at the piece-part and instrument levels to verify its performance and to define its operational characteristics to levels required to meet the science objectives. The tests and calibrations were carried out at ambient and vacuum chamber conditions. Also the instrument underwent extensive vibrational and thermal vacuum testing.

The ground testing and calibrations of NIRS were conducted primarily at the Institute of Space and Astronautical Science (ISAS), Japan. The tests at the piece-part level included measurements of detector linearity, responsivity as functions of wavelength and temperature

(Figure 3), dark current characteristics and spectral transmission properties of the grating (Figure 4).

Instrument-level calibrations of NIRS included measurements of the responsivity as a function of wavelength and FOV of each detector element (to verify detector linearity and alignment and to yield spectral resolution, spatial resolution, and flux calibration data), characterization of dark current levels for each detector element as a function of temperature, characterization of the level of spectral crosstalk on detector channels, and electronic performance characteristics of the detector arrays. Finally, measurements of the calibration targets and some of mineral and rock samples were made with the assembled NIRS instrument. The NIRS calibrations show that the detectors are linear and well aligned and that the instrument operates at very close to its design parameters for spatial and spectral resolution.

#### 4.1 Spectral Calibration

Spectral calibration was conducted in order to establish the wavelengths sensed by a detector for each of the 64 possible grating positions. That was performed by illuminating the instrument aperture with the monochromator, which is used in conjunction with an incandescent source and an integrating sphere. The signals from the detector arrays were recorded with the monochromator wavelength scanned in 100 nm increments over the first-order wavelength range. The spectral calibration was performed under the ambient temperature of 2°C. The results in the laboratory final test are shown in Figure 5. This figure shows the central wavelength of each of the detector arrays and the channel-to-wavelength relationship is expressed by:

$$\lambda = -23.56n + 2271.44(\text{nm}), \quad (1)$$

where  $n$  is the channel number between 1 to 64. The accuracy of this equation for linear fitting is approximately  $\pm 2$  nm.

Although the full range of the NIRS detector array is 751.8 to 2259.7 nm, it is further limited, however, to 850 to 2100 nm (channels 7-60). The lower six channels (channels 1-6, at 2248-2130 nm) are near or in the detector cutoff (Figure 3), making the effective upper bound for good signal-to-noise ratio (SNR) around 2100 nm for the signal level expected at Itokawa. The upper four channels of the InGaAs detector (channels 61-64, at 834-763 nm) register very low signal due to fall-off in detector responsivity and grism efficiency.

## 4.2 Radiometric Calibration

The radiometric response of the NIRS was determined in a number of tests by recording the detector response while viewing a laboratory calibrated field with a halogen lamp and a Spectralon reflectance target. The measurements used a 1 kW filament lamp with a quartz envelope containing halogen gas. The spectral radiance of this source has been calibrated by the Oriel Instruments and this calibration is directly traceable to the National Institute of Standards and Technology (NIST). The lamp was powered by regulated direct current at the prescribed amperage, measured using NIST-traceable instruments. In order to produce an extended source of known radiance, we used a Labsphere Spectralon standard, itself calibrated with traceability to NIST.

The per-channel DN-to-radiance conversion factor of the NIRS is shown in Figure 6. The response of the instrument was found to be linear and uncertainties of the NIRS absolute radiometric calibration were estimated to be approximately 10% in the effective wavelength range. Though the calibration was performed under the ambient condition, we applied the correction of atmospheric water vapor using the MODTRAN software. The NIRS radiometric calibrations showed that for radiances expected at Itokawa, a signal-to-noise ratio (SNR) in excess of 100 is easily attainable in 57 InGaAs channels (from 2 to 58) with nominal detector temperature of  $-15^{\circ}\text{C}$ . Since the detector temperature was maintained in an almost constant value in flight, except for caltarget observations, no temperature correction is required for the radiometric calibration.

## 4.3 Spatial Calibration

Alignment of the boresights of the Hayabusa scientific instruments relative to each other and to the nominal common boresight, the spacecraft  $-Z$  axis (the  $Z$  axis is perpendicular to the plane of Hayabusa's solar panels, and  $+Z$  direction on the spacecraft points toward the Sun with the spacecraft in its nominal orientation), were measured on ground, after spacecraft integration, using the reference optical cubes on each instrument. For NIRS, the accurate boresight vector was found to be inclined toward the spacecraft  $-Z$  axis with the Euler angles  $(-0.1140^{\circ}, -0.0012^{\circ}, 0.0^{\circ})$  and was verified the co-alignment with LIDAR. The FOV has rectangular shape with its sides along  $X$  and  $Y$  axes of the instruments frame and the angular size of  $0.1^{\circ}$ .

As these measurements were done under conditions of 1g and room temperature, conditions experienced by Hayabusa in space will distort the coalignment between

instruments slightly. Coalignment between the instruments was re-measured in flight and during the asteroid rendezvous.

## 5. In-flight Calibration

After launch, the NIRS performed a comprehensive series of in-flight tests to validate and supplement ground calibration data, and to characterize instrument stability, pointing, and co-alignment with other instruments under flight conditions. The in-flight observations of astronomical targets took place during the cruise phase before the arriving at Itokawa, with NIRS obtaining spatially resolved spectra of the Earth and Moon, and disk-integrated spectra of the Mars, Jupiter, and Saturn, including three bright stars.

### 5.1 Long-term Stability

The periodic onboard calibration-target observations in space assessed the long-term stability of radiometric and spectral characteristics. Figure 7 shows the results for the NIRS calibration-target observations at a constant detector temperature from after launch to the rendezvous, including a thermal vacuum test on ground. Figure 7a presents time series plots of relative responses for the selected NIRS channels normalized by the values obtained on May 16, 2003. Figure 7b in turn presents time series plots of the NIRS channels peaked in the LED spectra. The onboard calibrated LED generates a narrow spectrum centered at the specific wavelength of  $\sim 1.8 \mu\text{m}$ . Under a constant temperature condition, its peak wavelength does not shift beyond the NIRS spectral resolution.

Without short-term general increases as in Earth swingby and the arrival, the plots shows the gradual changes in NIRS channel responses up to  $\pm 3\%$ . The reason for this behavior is probably related to spectral alignment of the detector. Using the data of detector wavelength drift, we found that displacement of detector channels can generate such changes in the detector responses. The general high responsivity as seen in Earth swingby may be occurred by the lamp brightening due to the NIRS continuous operation. The rest of the overall time series corresponds to a gradual decay of the instrument primarily due to solar and cosmic ray radiation damage to the detectors and electronics. In addition, a general loss of 3-4% of NIRS response in the detector resulted from the launch.

The slight changes in instrument sensitivity over two years of in-flight operations were found, but the radiometric response had been highly stable on time scale of a few months. The linearities of NIRS detector response also were verified from the various exposure-time frames on the calibration-target observation. Thus, we found that differences in instrument

sensitivity of NIRS for the rendezvous phase fall within ~1% for overall effective detector channels.

## 5.2 Validation of Calibration Coefficients

Validation of the absolute calibration was performed through observations of the astronomical targets during the cruise. Figure 8 shows spectra of the Antares, Jupiter and Moon observed by the NIRS. For comparison, those spectra obtained by the ground-based telescopes are also shown (Lancon and Wood, 2000; Clark and McCord, 1979). The spectra show an overall close match between the NIRS data and the ground-based observations.

Stray light from outside of the FOV was not a major issue with NIRS since it was not identified in the pre-launch test with a blackbody cavity. However, significant stray reflections were found when NIRS had observed across the limb of Moon (Figure 8c and Figure 9). This may be due to the scattered light by the calibration lamp mounted on the aperture stop. The effect was dominant in the shorter wavelengths and required correction for proper calibration of the instrument. NIRS calibration did not incorporate a scattered light correction from pre-launch tests. The magnitude of out-of-field signal was quantified by acquiring swaths of spectra across the limb of Moon and Itokawa, during different orbits as the source of stray light changes in its size and illumination. These results will also be augmented by the results of the more controlled investigations of stray and scattered light conducted during pre-flight calibrations.

As for NIRS alignment and pointing, the co-alignment of NIRS with the AMICA and with respect to the spacecraft was determined from the simultaneous observations of bright stars as a point source. The other observation was attained during the Itokawa rendezvous phase. The NIRS had detected the reflected laser light of the LIDAR from the asteroid surface during the spacecraft descent (Abe et al., 2006). The LIDAR generates 1064-nm yttrium-aluminum-garnet-Nd (YAG-Nd) laser beam to measure distance by determining the time of flight for laser light to travel from the spacecraft to asteroid and return. The detected LIDAR spectra have shown the peak wavelength same as that obtained in prelaunch. Therefore, we found that there is no alteration of the NIRS spectral alignment from the prelaunch to final stage of the rendezvous phase. Moreover, LIDAR has a beamwidth of  $0.04^\circ \times 0.097^\circ$ , and such detection means that LIDAR boresight has been coaligned with NIRS as expected.

## 5.3 NIRS and AMICA Reflectance Comparison

Once spectra and images are calibrated and photometrically corrected to a uniform viewing geometry, the combination of spectra between the AMICA and NIRS can create a more complete near infrared spectrum to better characterize Itokawa's surface composition using absorption band features. To compare the absolute calibration between both instruments, we have calculated the geometric albedo (also known as the physical albedo) of Itokawa for each wavelength using the set of wavelength-dependent Hapke parameters derived from (Kitazato et al., 2008). The geometric albedo,  $A_g$ , is the weighted average of the normal albedo (the radiance factor of the surface at zero phase) over the illuminated area of the body (Hapke, 1993), and is written in the form

$$A_g = \left[ \int_{A(i)} r(e, e, 0) \mu dA \right] / \left[ \frac{1}{\pi} \int_{A(i)} \mu dA \right], \quad (2)$$

where  $r(i, e, \alpha)$  is the bidirectional reflectance of the surface,  $dA$  is the increment of area, and  $A(i)$  is the area of the illuminated surface of the body.

Figure 10 shows Itokawa's geometric albedo spectrum estimated with equation (2), including that value at visible wavelength ( $0.55 \mu\text{m}$ ) from the AMICA measurements (Ishiguro et al., 2007). In this figure, as an intermediary the disk-integrated visible to near-infrared spectra of Itokawa obtained by Binzel et al. (2001) and Tholen (2006) are displayed in accordance with AMICA. The prospective near-infrared albedos from the AMICA results appear to be approximately 7% larger than the real values measured by NIRS independently. Considering the uncertainties of absolute calibration for both instruments, this result can be regarded as a good agreement. As for the effect of a real asteroid shape on the geometric albedo, we found that its variation falls within  $\sim 1.5\%$  in the case of Itokawa. Although there is slight variations in geometric albedo due to different viewpoints, this cannot be a factor that fills a gap in absolute calibration between the NIRS and AMICA.

## 6. Summary

NIRS is a crucial component of the Hayabusa instrument complement needed to achieve the prime science objectives at the S type asteroid 25143 Itokawa. The instrument has been operational in space for over two and a half years and has collected abundant data from its onboard caltargets and observations in flight. NIRS has carried out numerous in-flight tests to validate its radiometric characteristics measured on-ground before launch and to characterize the instrument's long-term stability, pointing, and co-alignment with LIDAR. Test results

validate and refine coefficients to convert raw spectral data to scientifically useful calibrated data products. Main in-flight calibration results include the following: (1) Radiometric comparison of NIRS with its imaging companion AMICA is good. The two instruments agree to better than 10% for calculated radiance of Itokawa. Independent radiometric calibration of Antares and Jupiter with the ground-based telescopes yielded agreement better than 5%. (2) During the long cruise to Itokawa, the average responsivity of individual NIRS channels has gradually changed with up to 2% increase in the lower wavelength and about 2% decrease in the higher wavelengths. This change in responsivity might have resulted from a gradual displacement of detector arrays. (3) From limb scans of Moon and Itokawa, unexpected stray light was found to affect the NIRS spectra by up to 2%. In-flight experience allowed us to calibrate such effects. (4) The co-alignment of NIRS with respect to the other Hayabusa instruments has been determined.

### **Acknowledgments**

Development of the NIRS instrument, along with incorporation of necessary spacecraft accommodations, involved the work of many people. The authors would like to express their thanks to the entire NIRS team, whose efforts led to the success of this instrument on a very tight schedule.

## References

- Abe, M., Takagi, Y., Kitazato, K., Abe, S., Hiroi, T., Vilas, F., Clark, B. E., Abell, P. A., Lederer, S. M., Jarvis, K. S., Nimura, T., Ueda, Y., Fujiwara, A., 2006. Near-Infrared Spectral Results of Asteroid Itokawa from the Hayabusa Spacecraft. *Science* 312, 1334–1338.
- Abe, S., Mukai, T., Hirata, N., Barnouin-Jha, O. S., Cheng, A. F., Demura, H., Gaskell, R. W., Hashimoto, T., Hiraoka, K., Honda, T., Kubota, T., Matsuoka, M., Mizuno, T., Nakamura, R., Scheeres, D. J., Yoshikawa, M., 2006. Mass and Local Topography Measurements of Itokawa by Hayabusa. *Science* 312, 1344–1349.
- Binzel, R. P., Rivkin, A. S., Bus, S. J., Sunshine, J. M., Burbine, T. H., 2001. MUSES-C target asteroid (25143) 1998 SF36: A reddened ordinary chondrite. *Meteoritics and Planetary Science* 36, 1167–1172.
- Clark, R. N., McCord, T. B., 1979. Jupiter and Saturn - Near-infrared spectral albedos. *Icarus* 40, 180–188.
- Fujiwara, A., Mukai, T., Kawaguchi, J., Uesugi, K. T., 2000. Sample Return Mission to NEA : MUSES-C. *Advances in Space Research* 25, 231–238.
- Hapke, B., 1993. *Theory of reflectance and emittance spectroscopy*. Topics in Remote Sensing, Cambridge, UK: Cambridge University Press, —c1993.
- Ishiguro, M., Nakamura, R., Tholen, D. J., Hirata, N., Demura, H., Nemoto, E., Nakamura, A. M., Higuchi, Y., Sogame, A., Yamamoto, A., Kitazato, K., Yokota, Y., Kubota, T., Hashimoto, T., Saito, J., 2007. Calibration and Performance of Asteroid Multi-band Imaging Camera (AMICA) onboard Hayabusa Spacecraft. *Icarus* -, (submitted).
- Kitazato, K., Clark, B. E., Abe, M., Abe, S., Takagi, Y., Hiroi, T., Barnouin-Jha, O. S., Abell, P. A., Lederer, S. M., Vilas, F., 2008. Near-infrared spectrophotometry of Asteroid 25143 Itokawa from NIRS on the Hayabusa spacecraft. *Icarus* 194, 137–145.
- Kurucz, R., R. L., 1995. The solar irradiance by computation. *Proc. 17<sup>th</sup> Annual Conference Transmission Models*, Phillips Laboratory, Hanscom AFB, PL-TR-95-2060, G. P. Anderson et al. Eds., pp. 333-334.
- Lancon, A., Wood, P. R., 2000. A library of 0.5 to 2.5  $\mu$ m spectra of luminous cool stars. *A&AS* 146, 217–249.
- Okada, T., Shirai, K., Yamamoto, Y., Arai, T., Ogawa, K., Hosono, K., Kato, M., 2006. X-ray Fluorescence Spectrometry of Asteroid Itokawa by Hayabusa. *Science* 312, 1338–1341.
- Saito, J., Miyamoto, H., Nakamura, R., Ishiguro, M., Michikami, T., Nakamura, A. M., Demura, H., Sasaki, S., Hirata, N., Honda, C., Yamamoto, A., Yokota, Y., Fuse, T.,

Yoshida, F., Tholen, D. J., Gaskell, R. W., Hashimoto, T., Kubota, T., Higuchi, Y., Nakamura, T., Smith, P., Hiraoka, K., Honda, T., Kobayashi, S., Furuya, M., Matsumoto, N., Nemoto, E., Yukishita, A., Kitazato, K., Dermawan, B., Sogame, A., Terazono, J., Shinohara, C., Akiyama, H., 2006. Detailed Images of Asteroid 25143 Itokawa from Hayabusa. *Science* 312, 1341–1344.

**Table 1: NIRS Specifications**

Characteristic	Value
Spectral range	850 – 2100 nm
Spectral resolution	24 nm/channel
Detector element size	$30 \times 100 \mu\text{m}$
Number of detector elements	64
Grating ruling	75 grooves/mm
Slit size	$70 \times 70 \mu\text{m}$
Field of view	$0.1^\circ \times 0.1^\circ$
Aperture	$\phi 27.2 \text{ mm}$
Imaging interval	65.536 ms
Integration time	0.256 – 57.344 ms
Shutter driving	7.63 Hz (131.072 ms)
Size	$336 \times 165 \times 100 \text{ mm}$ (NIRS-S)
Mass	1.53 kg (NIRS-S)
Power	9.50 W (NIRS-S), 0.45 W (NIRS-E)

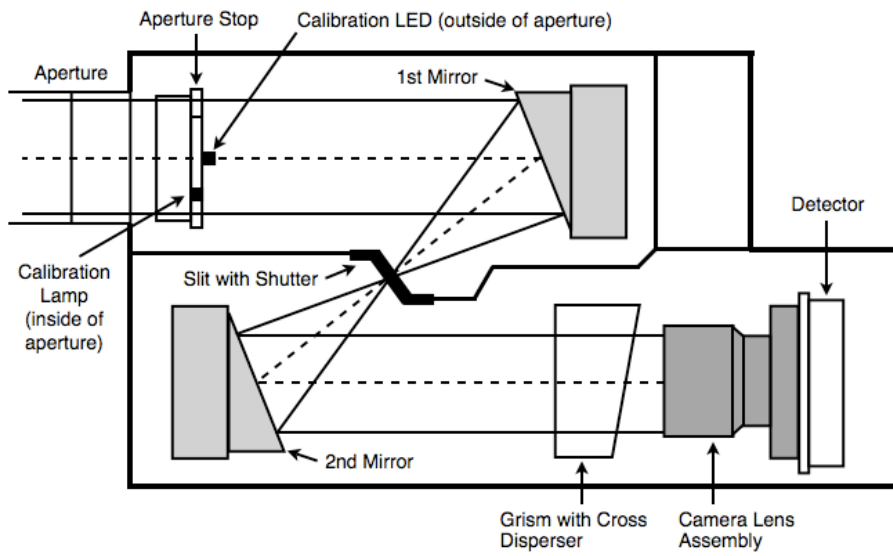


**Figure 1:** Schematic optical design of the NIRS.

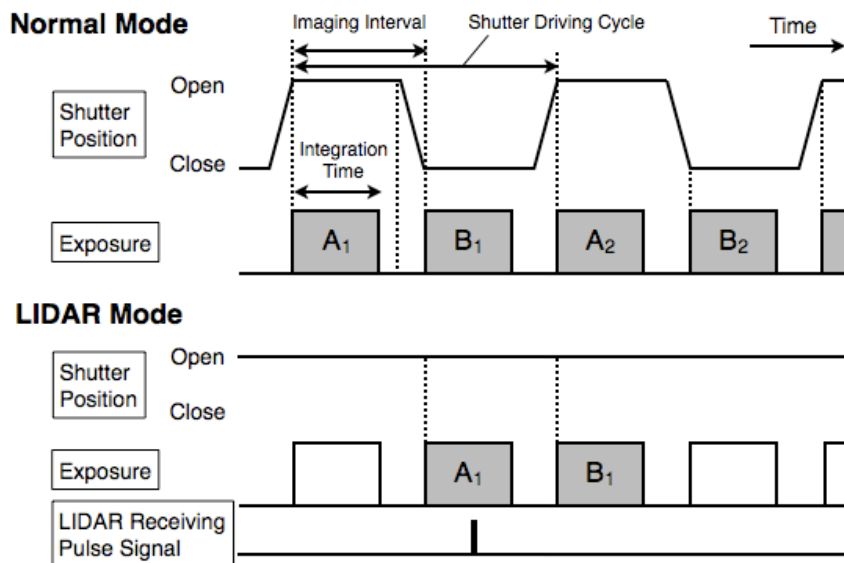


**Figure 2:** NIRS timing chart.

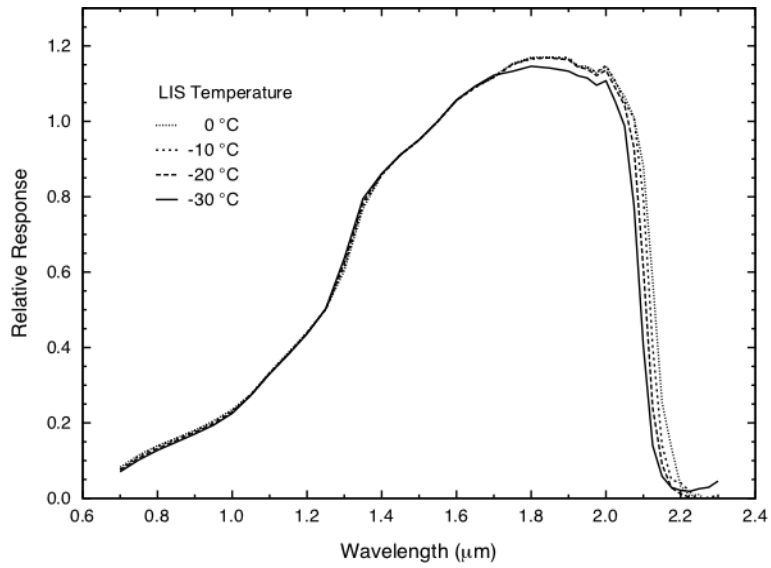


**Figure 3:** Spectral responsivity of InGaAs detector array depending on temperature.

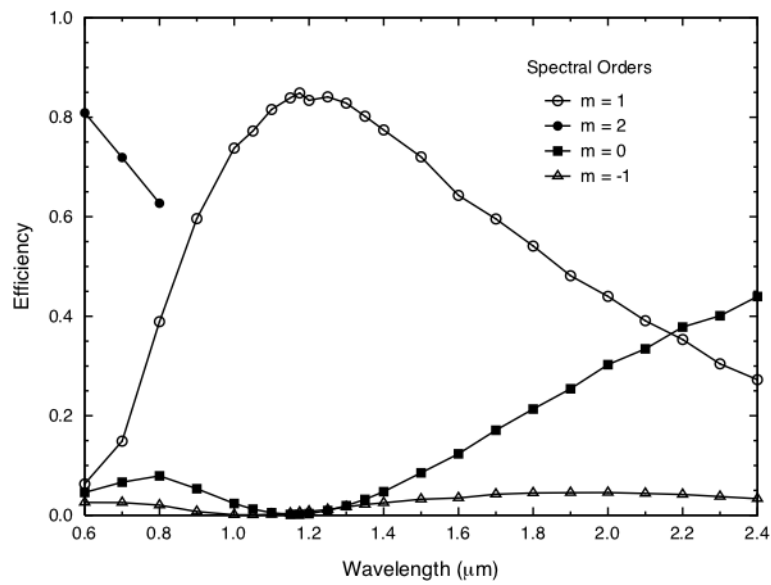


**Figure 4:** The measured grism efficiency for different spectral orders.

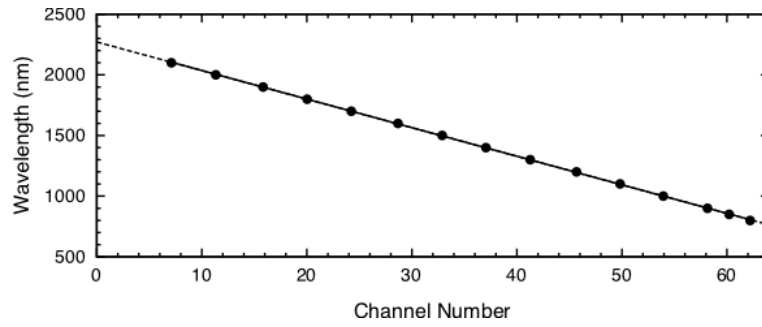


**Figure 5:** Spectral calibration data and linear regression.

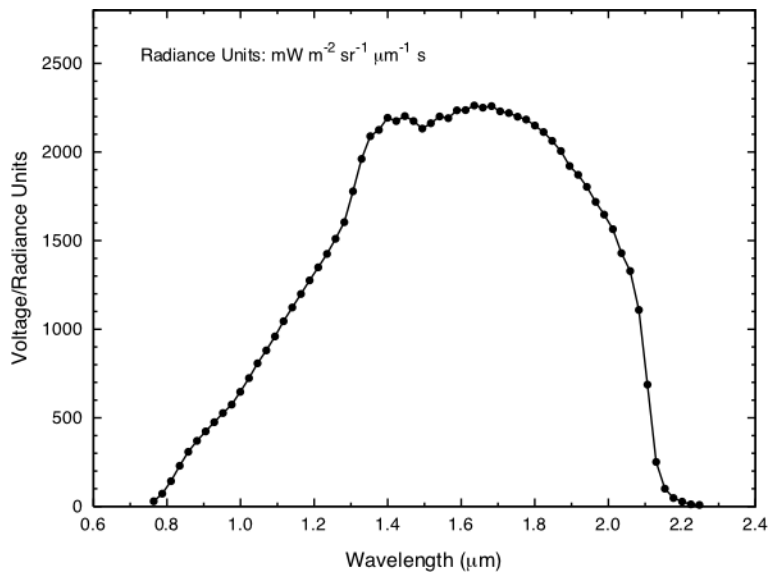


**Figure 6:** The radiometric calibration of the NIRS determined from laboratory tests, corresponding to a field filling source.

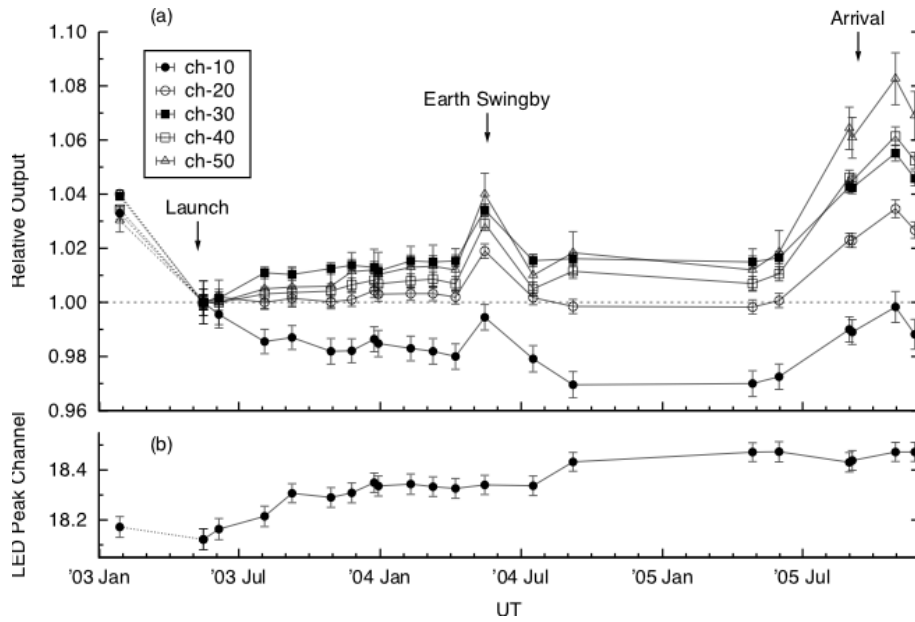


**Figure 7:** Time series plots for (a) the NIRS channel responses in lamp observation and (b) the peak channels in LED observation.

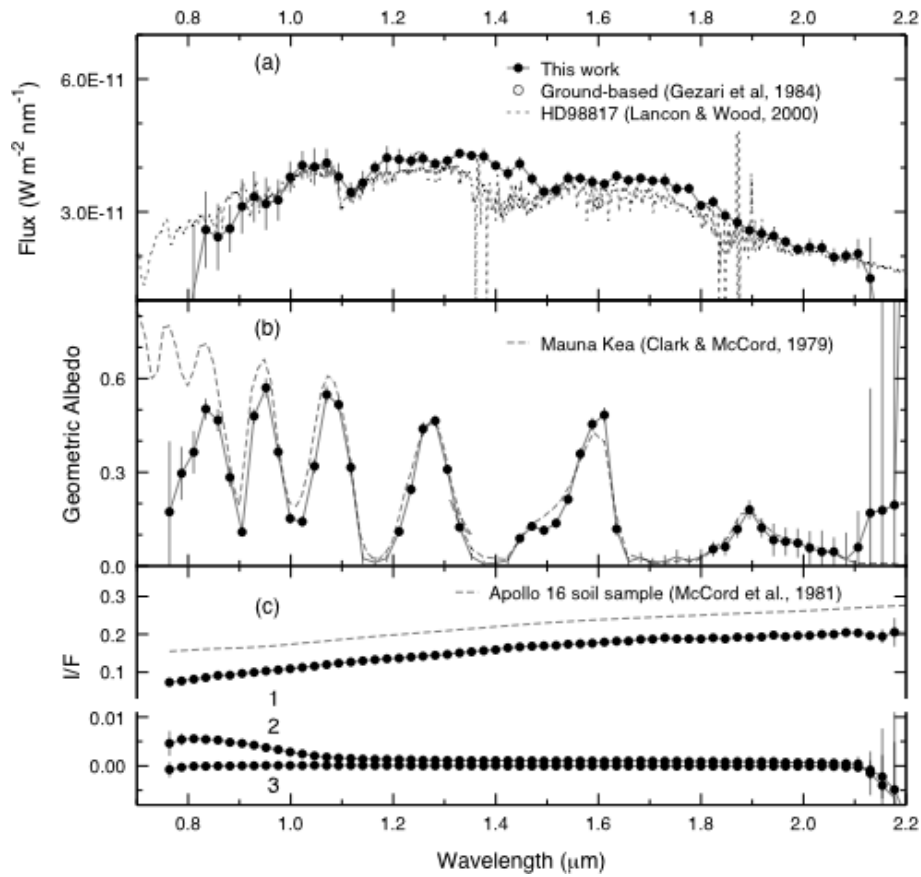


**Figure 8:** Representative NIRS spectra obtained from in-flight measurements: (a) Antares, (b) Jupiter, (c) Moon. The spectra used for comparison were taken by the ground-based telescopes (Lancon and Wood, 2000; Clark and McCord, 1979).

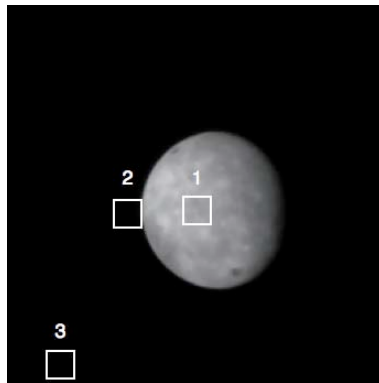


**Figure 9:** The image of Moon taken by the AMICA shows the relative position of the individual observation of NIRS. The number in NIRS FOV frames corresponds to that in Figure 8 respectively.

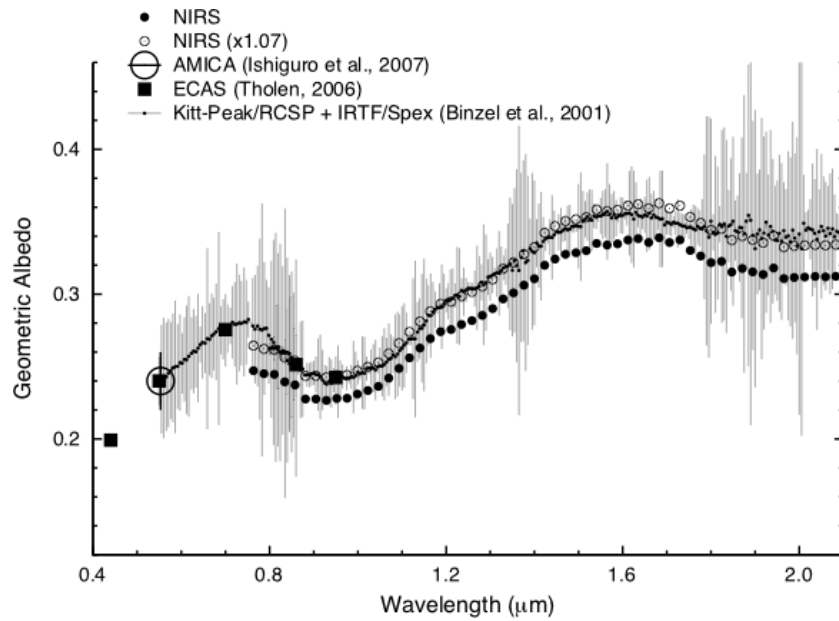


**Figure 10:** Comparison of the derived geometric albedo of Itokawa between the NIRS and AMICA. The value at V-band ( $0.55 \mu\text{m}$ ) has been estimated by AMICA (Ishiguro et al., 2007). As an intermediary the visible to near-infrared spectra of Itokawa obtained from the ground-based observations by Binzel et al. (2001) and Tholen (2006) are plotted with normalized at the value of AMICA's V-band.